Energy 44 (2012) 902–910

Contents lists available at SciVerse ScienceDirect

Energy

journal homepage: www.elsevier.com/locate/energy

# Thermodynamic optimization of a Stirling engine

M.C. Campos [a], J.V.C. Vargas [a,*], J.C. Ordonez [b]

[a] Programa de Pós-Graduação em Engenharia e Ciência dos Materiais, PIPE, and Departamento de Engenharia Mecânica, Universidade Federal do Paraná, UFPR, CP 19011, 81531-980 Curitiba, PR, Brazil
[b] Department of Mechanical Engineering and Center for Advanced Power Systems, Florida State University, Tallahassee, FL 32310-6046, USA

ARTICLE INFO

*Article history:*
Received 4 November 2011
Received in revised form
9 April 2012
Accepted 30 April 2012
Available online 8 June 2012

*Keywords:*
Stirling engines
Thermodynamic optimization
Heat engines

ABSTRACT

A Stirling engine configuration consisting of two cylinders, a regenerator and a sliding disc actuating mechanism ("swashplate") is considered in this paper. A mathematical model, which combines fundamental and empirical correlations, and principles of classical thermodynamics, mass and heat transfer accounting for variable heat transfer coefficients, is developed. The proposed model is then utilized to simulate numerically the system transient and steady state response under different operating and design conditions. A system global optimization for maximum performance in the search for optimal parameters that lead to maximum cycle efficiency is performed with low computational time. Appropriate dimensionless groups are identified and the results presented in normalized charts for general application. The numerical results show that the two-way maximized system efficiency, $\eta_{max,max}$, occurs when two system characteristic parameters, the ratio between the total swept volume during the expansion, and the total swept volume, $\varphi$, and the ratio between the heat transfer area of the hot side heat exchanger and the total heat exchange area, y, are optimally selected, i.e., $(\varphi, y)_{opt} \cong (0.5, 0.4)$. The two-way maximized cycle efficiency found with respect to the optimized parameters is sharp, in the sense that a 225% variation of the calculated efficiency values was observed within the range of tested configurations in this study, and "robust" (i.e., relatively insensitive) to the variation of several parameters, thus stressing the importance to be considered in actual design. It is also found that the twice-maximized cycle efficiency and the total engine work output increase monotonically with the temperature of the hot source, $T_h$. As a result, the model is expected to be a useful tool for simulation, design, and optimization of Stirling engines.

© 2012 Elsevier Ltd. All rights reserved.

## 1. Introduction

Stirling engines are classified as thermal (or heat) engines within the theoretical thermodynamic framework. The Stirling engine thermodynamic cycle displays a theoretical thermal efficiency equal to the Carnot limit [1]. However, the heat transfer in this ideal limit must occur isothermally and reversibly, which demands infinite time, therefore, zero power is observed in the efficiency limit, $1-T_c/T_h$, in which $T_h$ is the temperature of the hot reservoir and $T_c$ the temperature of the cold reservoir. The mechanical difficulty to accomplish the ideal volume variation in the Stirling cycle is also responsible to separate the real from the ideal cycle.

A previous work by Curzon and Ahlborn [2] showed that the efficiency of a Carnot engine with a finite heat transfer time depends only upon the temperatures $T_h$ and $T_c$, and is given by:

$$\eta_{max} = 1 - \sqrt{\frac{T_c}{T_H}} \tag{1}$$

As a result, the Stirling engine is a promising alternative, taking into account that it is an external combustion engine with possibilities for better combustion control and the potential to use multiple fuels. Therefore, with proper design, Stirling engines are expected to be less expensive and less polluting than Diesel engines and even gas turbines.

The expectation of achieving thermal efficiencies close to the Carnot limit developed interest in the Stirling engine among researchers. Several authors have published theoretical and experimental studies on that possibility. Reader and Hooper [3] presented experimental measurements and analyses of Stirling engines. Uriel and Berchowitz [4] described analytically different

* Corresponding author. Dept. of Mechanical Engineering, Universidade Federal do Parana, Caixa Postal 19011, Curitiba, PR CEP 81531-980, Brazil. Tel.: +55 41 3361 3307.
*E-mail address:* jvargas@demec.ufpr.br (J.V.C. Vargas).

0360-5442/$ – see front matter © 2012 Elsevier Ltd. All rights reserved.
doi:10.1016/j.energy.2012.04.060

actuation mechanisms used in Stirling engines and presented mathematical models for the thermodynamic simulation of the cycle considering variable heat transfer coefficients and the pressure drop in tubular heat exchangers of circular cross-section.

A finite time thermodynamic analysis of the Stirling cycle was presented by Ladas [5] with a sinusoidal volume variation and so called Beta configuration. The mass and energy balance equations were nondimensionalized and the maximum efficiency obtained was 14%.

Finite time thermodynamics, endoreversible and simplified models have been used for Stirling engine optimization. For example: Blank and Wu [6] studied the power output and thermal efficiency of a finite time, optimized, extra-terrestrial, solar-radiant Stirling heat engine, in which the heat source and sink were assumed to have infinite heat-capacity rates, obtaining expressions for optimum power and efficiency at optimum power; heat pumps based on the reversed Stirling cycle were also studied [7] using a simplified model, which allowed a first optimization of real gas cycles, showing that efficiencies much higher than those achievable with an ideal gas, and similar to those of vapor–compression cycles can be obtained; a finite time thermodynamic optimization of a Stirling engine was performed by Popescu et al. [8], considering an endo- and exo-irreversible cycle, i.e., accounting for general irreversibilities, finding optimum operating conditions leading to maximum power output in good agreement with experimental data; Erbay and Yavuz [9] studied the Stirling heat engine operating in a closed regenerative thermodynamic cycle finding the maximum power density and efficiency, in addition to the compression ratio at maximum power density; Bhattacharyya and Blank [10] reported major theoretical considerations concerning the design of an endoreversible Stirling cycle with ideal regeneration; Senft [11] used the classic Schmidt thermodynamic model (isothermal model) for Stirling engines and revisited the problem of identifying optimal engine geometry; Rogdakis et al. [12] performed the optimization of stable operation of the Stirling cycle in the free piston configuration, and for simplicity reasons used the Schmidt analysis; a thermoeconomic optimization of an irreversible Stirling cryogenic refrigerator cycle was presented by Tyagi et al. [13] finding that the effect of regenerative effectiveness is more than those of the other parameters on all the performance parameters of the cycle, and Mathieu et al. [14] performed the pre-sizing of the thermal storage and the solar receiver area of a thermodynamic micro power station and searched for possible optimum temperature levels. However, all such analyses were performed with steady state models.

Two studies were found in the literature [15,16] that utilized dynamic models which included thermal losses to optimize the performance and design parameters of the Stirling engine, after experimental validation against data obtained from the General Motor GPU-3 Stirling engine prototype, showing significant engine efficiency increase with respect to the original configuration, i.e., from 39% to 51% increase. Although the study was dimensional and specific to the GPU-3 Stirling engine, it shows the importance of using dynamic models for engine optimization in order to produce more realistic results. For example, Karabulut [17] analyzed a free piston Stirling engine with a dynamic model, which made possible to show that the closed cycle performs a stable operation within a small range of the hot end temperature and damping coefficient of the piston motion that could be partially enlarged by inverting the engine into an open-cycle engine.

The bibliographic review shows that there is a lack of studies on the thermodynamic optimization of Stirling engines with dynamic, dimensionless and more elaborated mathematical models. Therefore, this paper's objective is to present a dimensionless dynamic mathematical model to simulate the thermodynamic behavior of a Stirling engine in the transient regime as a function of geometrical and operating parameters relevant to the engine design. Appropriate dimensionless groups are introduced in order to present normalized simulation results for general engineering application. Acknowledging the finite availability of space in any engineering project, a constraint accounting for the total volume occupied by the engine is imposed. The mathematical model is then utilized to optimize some engine operating and design parameters for maximum cycle efficiency.

## 2. Mathematical model

Fig. 1 depicts a schematic diagram of the Stirling engine configuration considered in this work, consisting of: two cylinders, the hot and cold side heat exchangers, the regenerator and the sliding disc actuating mechanism ("swashplate"). One possible

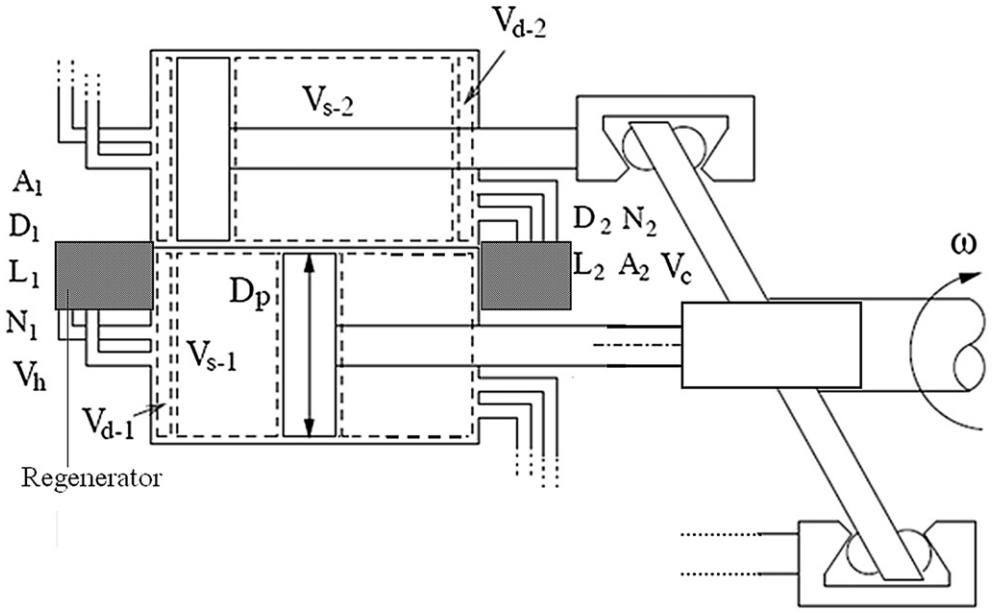


**Fig. 1.** Schematic representation of the sliding disk mechanism ("swashplate") and cylinders-regenerator unit consisting of a hot space, a cold space and a regenerator.

arrangement is a four-cylinder swashplate-drive double-acting engine (e.g., the Ford-Philips 4-215 engine [4]), which is the one considered in this work, i.e., each piston is responsible for the compression process in one side and the expansion process in the other side.

The proposed thermodynamic model considers three control volumes: hot space (CV-1), cold space (CV-2), and the regenerator (CV-3). The model is dynamic, therefore in the analysis, temperatures in the three control volumes vary with respect to time, and volume in CV-1 and CV-2 also vary in time due to piston-displacement, but CV-3 undergoes constant volume processes since the regenerator volume is constant. The basic assumptions are: uniform temperatures in the control volumes, negligible pressure drops across the regenerators and heat exchangers, and the working fluid is treated as an ideal gas. The idea is to model the engine as an assembly of modules, like the one shown in Fig. 1, with identical thermodynamic performance. It is therefore sufficient to analyze one module and obtain the total engine power (or work) multiplying the power of one module by the engine's number of modules.

The pistons are driven by the swashplate mechanism illustrated in Fig. 1, resulting in a pure sinusoidal reciprocating motion having a phase difference between the adjacent pistons, given by the angle between pistons, $\alpha$. Therefore, the total expansion volume, $V_1$, and the total compression volume, $V_2$, vary in time, and are calculated by [4]:

$$V_1 = V_h + V_{d-1} + \frac{V_{s-1}}{2}[1 + \cos(\omega t + \alpha)] \quad (2)$$

$$V_2 = V_c + V_{d-2} + \frac{V_{s-2}}{2}[1 + \cos(\omega t)] \quad (3)$$

where $V_h$ and $V_c$ represent the volume occupied by the hot and cold heat exchangers respectively, $V_{d\text{-}1}$ and $V_{d\text{-}2}$ represent the dead volumes for expansion and compression, and $V_{s\text{-}1}$ and $V_{s\text{-}2}$ the total swept volumes for expansion and compression for each cylinder.

The phase angle between sets of cylinders, $\alpha$, is shown in Fig. 2a, and the total number of cylinders, results directly from its value. For example, for the swashplate mechanism considered in this work, with $\alpha = 90^\circ$, the result is an engine with 4 cylinders and 4 modules as shown schematically in Fig. 2b.

In Equations (2) and (3) the term $(V_h + V_{d\text{-}1})$ represents the total dead expansion volume and $(V_c + V_{d-2})$ the total dead compression volume.

The time derivatives of the expansion and compression volumes for the sliding disk mechanism are given by:

$$\frac{dV_1}{dt} = -\frac{V_{s-1}}{2}\,\omega\,\sin(\omega t + \alpha) \quad (4)$$

$$\frac{dV_2}{dt} = -\frac{V_{s-2}}{2}\,\omega\,\sin(\omega t) \quad (5)$$

The volumes $V_h$ and $V_c$ are functions of the heat exchanger geometry as follows:

$$V_h = \frac{N_1 \cdot L_1 \cdot \pi \cdot D_1^2}{4} \quad (6)$$

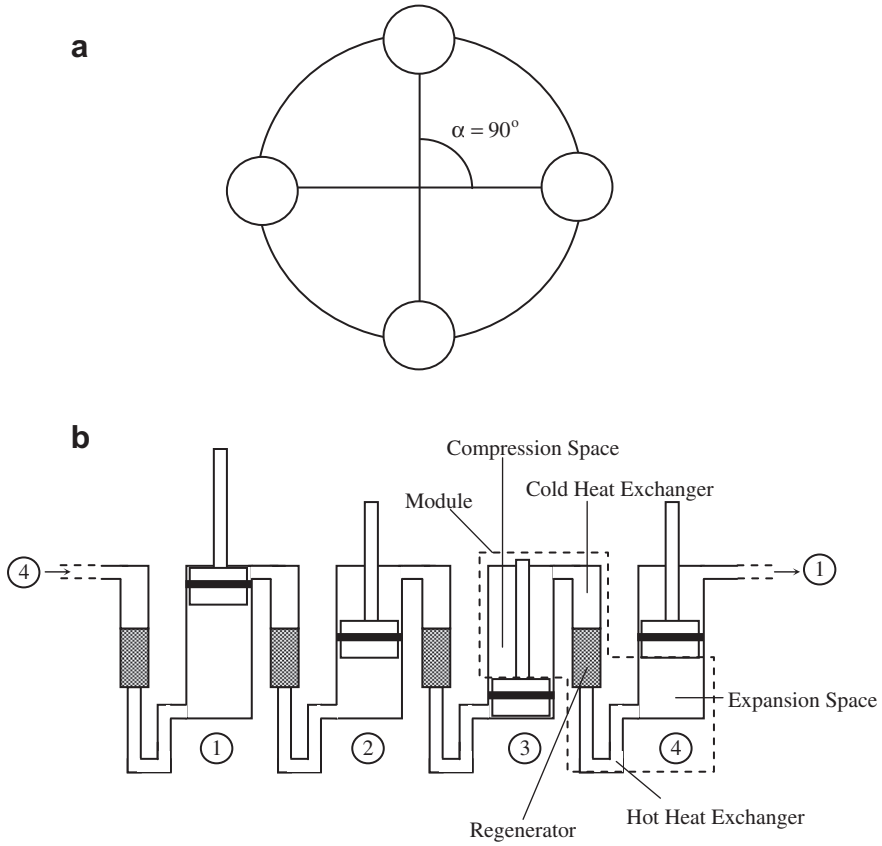


**Fig. 2.** (a) Illustration of the phase angle between piston units, $\alpha$, and (b) The schematic representation of the components of one module in the double-acting swashplate Stirling engine considered in this work.

$$V_c = \frac{N_2 \cdot L_2 \cdot \pi \cdot D_2^2}{4} \tag{7}$$

where $N_1$, $L_1$ and $D_1$ are the number, length, and diameter of the tubes in the hot side heat exchanger, respectively, and $N_2$, $L_2$ and $D_2$ are the number, length and diameter of the tubes in the cold side heat exchanger.

Assuming uniform internal pressure, $p$, and neglecting the volume occupied by the gas inside the regenerator, the mass and energy conservation equations for the expansion and compression volumes state that:

$$\frac{dm_1}{dt} = \dot{m} \tag{8}$$

$$c_v \frac{d(m_1 T_1)}{dt} = \dot{Q}_1 - p\frac{dV_1}{dt} + c_p \dot{m} T_{c-1} \tag{9}$$

$$\frac{dm_1}{dt} + \frac{dm_2}{dt} = 0 \tag{10}$$

$$c_v \frac{d(m_2 T_2)}{dt} = \dot{Q}_2 - p\frac{dV_2}{dt} + c_p \dot{m} T_{c-2} \tag{11}$$

where $T_{c-1}$ and $T_{c-2}$ are conditional temperatures that depend on the gas flow direction inside the engine and on the heat exchange in the regenerator; $m_1$ and $T_1$ are the mass and temperature in the expansion volume, respectively; $m_2$ and $T_2$ are the equivalent quantities in the compression volume; $c_p$ and $c_v$ are the working fluid specific heat at constant pressure and at constant volume, respectively, and $\dot{Q}_1$ and $\dot{Q}_2$ are the heat transfer rates in the hot and cold side heat exchangers, respectively.

Combining the differential forms of the equations of state for each control volume, i.e., $d(m_i T_i)/dt = 1/R(p(dV_i/dt) + V_i(dp/dt))$ for $i = 1, 2$, referring to CV-1 and CV-2, respectively, with Equations (9)–(11), it is possible to obtain differential equations to compute the internal pressure and the mass in the expansion volume as follows:

$$\frac{dp}{dt} = \frac{(\gamma - 1)\left(\frac{\dot{Q}_1}{T_{c-1}} + \frac{\dot{Q}_2}{T_{c-2}}\right) + p\gamma\left(\frac{1}{T_{c-1}}\frac{dV_1}{dt} + \frac{1}{T_{c-2}}\frac{dV_2}{dt}\right)}{\frac{V_1}{T_{c-1}} + \frac{V_2}{T_{c-2}}} \tag{12}$$

$$\frac{dm_1}{dt} = \left(\frac{V_1}{R\gamma T_{c-1}}\right)\frac{dp}{dt} + \left(\frac{p}{RT_{c-1}}\right)\frac{dV_1}{dt} - \frac{\dot{Q}_1}{c_p T_{c-1}} \tag{13}$$

where $R$ is the gas constant and $\gamma$ the working fluid specific heats ratio $c_p/c_v$.

The heat transfer rate between the regenerator matrix and the gas is computed as follows:

$$\dot{Q}_R = m_R c_R \frac{dT_m}{dt} = c_p[a(T_2 - T_R) + b(T_R - T_1)]\frac{dm_1}{dt} \tag{14}$$

where the coefficients $a$ and $b$ alternate between 0 and 1 according to the flow direction. $T_R$ is the temperature of the gas leaving the regenerator; $T_m$ the temperature of the regenerator matrix $m_R$ the matrix mass, and $c_R$ the regenerator specific heat.

The values of the coefficients $a$ and $b$ are given by:

$$(a = 1) \text{ and } (b = 0) \text{ for } \frac{dm_1}{dt} > 0 \tag{15}$$

and

$$(a = 0) \text{ and } (b = 1) \text{ for } \frac{dm_1}{dt} < 0 \tag{16}$$

The temperature $T_R$ is found using the regenerator effectiveness, $\varepsilon$, which is also a function of the flow direction and the temperatures $T_1$, $T_2$ and $T_m$, in the following way:

$$T_R = a[T_2 + \varepsilon(T_m - T_2)] + b[T_1 + \varepsilon(T_m - T_1)] \tag{17}$$

The conditional temperatures, $T_{c-1}$ and $T_{c-2}$ are, therefore given by:

$$T_{c-1} = a \cdot T_R + b \cdot T_1 \tag{18}$$

$$T_{c-2} = a \cdot T_2 + b \cdot T_R \tag{19}$$

Equation (14) is rewritten, solving for $dT_m/dt$:

$$\frac{dT_m}{dt} = \frac{c_p \varepsilon}{m_R c_R}[a(T_2 - T_m) + b(T_m - T_1)]\frac{dm_1}{dt} \tag{20}$$

The heat transfer rates in the expansion and compression volumes are obtained as follows:

$$\dot{Q}_1 = h_1 A_1 \cdot (T_h - T_1) \tag{21}$$

$$\dot{Q}_2 = h_2 A_2 \cdot (T_c - T_2) \tag{22}$$

where $h_1$ and $h_2$ are the heat transfer convection coefficients, $A_1$ and $A_2$ the heat transfer areas in the expansion and compression volumes, respectively. The heat transfer areas $A_1$ and $A_2$, are given by:

$$A_1 = N_1 \cdot L_1 \cdot \pi \cdot D_1 \tag{23}$$

$$A_2 = N_2 \cdot L_2 \cdot \pi \cdot D_2 \tag{24}$$

The convection heat transfer coefficients vary during the engine operating cycle due to the variation in the gas mass flow rates and they are calculated using Colburn's correlation [18] as follows:

$$h = \frac{0.023\ \mathrm{Re}_D^{4/5}\mathrm{Pr}^{1/3}\ k}{D} \tag{25}$$

where $k$ is the gas thermal conductivity; Pr is the Prandtl number, and $\mathrm{Re}_D$ is the Reynolds number based on the tube internal diameter.

In order to proceed with the optimization of engine parameters for maximum efficiency, a volume constraint is introduced, to characterize the engine's finite space availability:

$$V^* = V_C + V_h + V_{d-1} + V_{d-2} + V_{S-1} + V_{S-2} \tag{26}$$

where $V^*$ is a reference volume, kept fixed during the optimization procedure.

In order to nondimensionalize the mathematical model, the following scales are used:

$$\begin{aligned} t^* &= \frac{2.\pi}{\omega} \quad D^* = D_p \quad A^* = \frac{V^*}{D^*} \\ h^* &= \frac{m_t c_v}{t^* A^*} \quad p^* = \frac{m_t R T_c}{V^*} \quad T^* = T_c \quad M^* = \frac{m_R c_R}{m_t c_p} \end{aligned} \tag{27}$$

The dimensionless variables are therefore defined by:

$$\begin{aligned} \tilde{t} &= \frac{t}{t^*} \quad \tilde{T}_i = \frac{T_i}{T^*} \quad \tilde{p} = \frac{p}{p^*} \\ \tilde{m}_i &= \frac{m_i}{m_t} \quad \tilde{V}_1 = \frac{V_1}{V^*} \quad \tilde{V}_2 = \frac{V_2}{V^*} \end{aligned} \tag{28}$$

Additionally, the following dimensionless parameters for the engine are used:

$$\tilde{h}_i = \frac{h_i}{h^*} \quad \tilde{D}_i = \frac{D_i}{D^*} \quad \tilde{A}_i = \frac{A_i}{A^*}$$
$$\tilde{V}_i = \frac{V_i}{V^*} \quad \tilde{L}_i = \frac{L_i}{D^*} \quad \tilde{T}_h = \frac{T_h}{T_c} \tag{29}$$

The index $i$, in Equations (28) and (29), refers to the points in s−1, s−2, d−1, d−2, c, h, 1, 2, m, R, c−1, c−2 in Fig. 1, representing the expansion swept volume, the compression swept volume, the dead expansion volume, the dead compression volume, cold side heat exchanger, hot side heat exchanger, expansion space, compression space, regenerator matrix, fluid in the regenerator, conditional temperature in the expansion space, and conditional temperature during compression, respectively, in the applicable variables.

Substituting the dimensionless variables into Equations (12), (13) and (20) we obtain:

$$\frac{d\tilde{p}}{d\tilde{t}} = \frac{\left(\frac{\tilde{h}_1\cdot\tilde{A}_1\cdot\left(\tilde{T}_h-\tilde{T}_1\right)}{\tilde{T}_{c-1}}+\frac{\tilde{h}_2\cdot\tilde{A}_2\cdot\left(1-\tilde{T}_2\right)}{\tilde{T}_{c-2}}\right)+\tilde{p}\gamma\left(\frac{1}{\tilde{T}_{c-1}}\frac{d\tilde{V}_1}{d\tilde{t}}+\frac{1}{\tilde{T}_{c-2}}\frac{d\tilde{V}_2}{d\tilde{t}}\right)}{\frac{\tilde{V}_1}{\tilde{T}_{c-1}}+\frac{\tilde{V}_2}{\tilde{T}_{c-2}}} \tag{30}$$

$$\frac{d\tilde{m}_1}{d\tilde{t}} = \left[\tilde{V}_1\frac{d\tilde{p}}{d\tilde{t}}+\gamma\tilde{p}\frac{d\tilde{V}_1}{d\tilde{t}}-\tilde{h}_1\cdot\tilde{A}_1\cdot\left(\tilde{T}_h-\tilde{T}_1\right)\right]\frac{1}{\gamma\cdot\tilde{T}_{c-1}} \tag{31}$$

$$\frac{d\tilde{T}_m}{d\tilde{t}} = \frac{\varepsilon}{M^*}\left[a\left(\tilde{T}_2-\tilde{T}_m\right)+b\left(\tilde{T}_m-\tilde{T}_1\right)\right]\frac{d\tilde{m}_1}{d\tilde{t}} \tag{32}$$

The dimensionless temperatures $\tilde{T}_R$, $\tilde{T}_{c-1}$ and $\tilde{T}_{c-2}$ are defined as follows:

$$\tilde{T}_R = a\left[\tilde{T}_2+\varepsilon\left(\tilde{T}_m-\tilde{T}_2\right)\right]+b\left[\tilde{T}_1+\varepsilon\left(\tilde{T}_m-\tilde{T}_1\right)\right] \tag{33}$$

$$\tilde{T}_{c-1} = a\cdot\tilde{T}_R+b\cdot\tilde{T}_1 \tag{34}$$

$$\tilde{T}_{c-2} = a\cdot\tilde{T}_2+b\cdot\tilde{T}_R \tag{35}$$

Several parameters, related to the volume distribution are needed to study and optimize the engine: $\sigma$, $\varphi$, $\psi$, $x$, and $\beta$. This last parameter is introduced to study the influence in the engine performance of the relation between the reference volume and the piston diameter. Additionally, the following parameters related to the heat exchangers geometry are used: $y$, $Z_1$, $Z_2$, and $w$. The nomenclature fully presents their definitions and mathematical expressions.

It is possible to show that several parameters defined in the previous paragraph have the following relationships:

$$w = \frac{y\cdot(1-x)}{x(1-y)} \tag{36}$$

$$\left(\tilde{V}_h+\tilde{V}_c\right) = \psi(1-\sigma) \tag{37}$$

$$\tilde{D}_1 = \frac{4\left(\tilde{V}_h+\tilde{V}_c\right)}{[y+(1-y)w]\tilde{A}} \tag{38}$$

Using Eucken's correlation, $k = \mu(c_p + 5.R/4)$ [19] for the gas thermal conductivity and $Re_d = \dot{m}\,L\,D/(\mu\,V)$ for the Reynolds number, as a function of the mass flow rate, tube length, tube diameter and volume occupied by the working fluid in the heat exchanger, it is possible to obtain expressions for $\tilde{h}_1\cdot\tilde{A}_1$ and $\tilde{h}_2\cdot\tilde{A}_2$ as functions of the dimensionless mass flow rate, $d\tilde{m}_1/d\tilde{t}$, the gas properties and the dimensionless parameters previously defined:

$$\tilde{h}_1\cdot\tilde{A}_1 = \frac{\gamma^{1/3}(9\gamma-5)^{2/3}}{27.39}\left[\left(\frac{\mu V^* t^*}{m_t D_p^2}\right)\left(\frac{Z_1^4 y\tilde{A}}{\tilde{D}_1}\right)\right]^{1/5}\left(\left|\frac{d\tilde{m}_1}{d\tilde{t}}\right|\right)^{4/5} \tag{39}$$

$$\tilde{h}_2\cdot\tilde{A}_2 = \frac{\gamma^{1/3}(9\gamma-5)^{2/3}}{27.39}\left\{\left(\frac{\mu V^* t^*}{m_t D_p^2}\right)\left[\frac{Z_2^4(1-y)\tilde{A}}{w\tilde{D}_1}\right]\right\}^{1/5}\left(\left|\frac{d\tilde{m}_1}{d\tilde{t}}\right|\right)^{4/5} \tag{40}$$

The dimensionless network, $\tilde{W}$, and heat transfer, $\tilde{Q}_1$, per cycle, are found by:

$$\frac{d\tilde{W}}{d\tilde{t}} = \tilde{p}\left(\frac{d\tilde{V}_1}{d\tilde{t}}+\frac{d\tilde{V}_2}{d\tilde{t}}\right) \tag{41}$$

$$\frac{d\tilde{Q}_1}{d\tilde{t}} = \tilde{h}_1\cdot\tilde{A}_1\left(\tilde{T}_h-\tilde{T}_1\right) \tag{42}$$

Assigning a zero value to $\tilde{W}$ and $\tilde{Q}_1$ at the beginning of the cycle, the total dimensionless work $\tilde{W}_t$ and heat transfer $\tilde{Q}_{1-t}$ during the engine cycle are represented by the values of $\tilde{W}$ and $\tilde{Q}_1$ respectively, when $\tilde{t} = 1$ (end of the cycle).

The cycle efficiency, $\eta$, is therefore defined using $\tilde{W}_t$ and $\tilde{Q}_{1-t}$:

$$\eta = (\gamma-1)\frac{\tilde{W}_t}{\tilde{Q}_{1-t}} \tag{43}$$

## 3. Numerical method and error analysis

Equations (30)–(32) define a system of three ordinary differential equations that was solved numerically with an adaptive time step fourth-fifth order Runge-Kutta method [20], together with Equations (33)–(35), (39), (40) in the dimensionless time interval $(0 \le \tilde{t} \le 1)$. As a result, the thermodynamic properties of the gas during an operating cycle were obtained. Such dimensionless time interval is the time required to complete an engine cycle.

For each set of geometric and operating parameters, the system is solved iteratively for correct boundary conditions, i.e., requiring that the unknowns $\tilde{p}$, $\tilde{m}_1$ and $\tilde{T}_m$ computed at the end of the cycle ($\tilde{t} = 1$) do not differ from their values at the beginning of the cycle since the working fluid is in the same thermodynamic state. This is done by computing a cycle relative error and satisfying the following convergence criterion [21]:

$$\varepsilon_{cycle} = \frac{|u_{j+1} - u_j|}{u_j} \leq tol \tag{44}$$

where $u = \tilde{p}, \tilde{m}_1$ or $\tilde{T}_m$, tol is a convergence tolerance limit (e.g., 0.01 or 1%), and $j \geq 0$ is the iteration counter. All three unknowns need to be tested according to the criterion of Equation (44) to ensure convergence.

The process for finding correct boundary conditions starts from initial values estimated at the beginning of the cycle in the first iteration, which are replaced by the calculated values at the end of the first iteration, to start the second iteration and so on, until convergence is attained. In this work, the selected point to start the process computing the cycle relative error according to Equation (44) was the beginning of compression, with estimated initial values at $j = 0$, $\tilde{p}_0 = 1$, $\tilde{T}_{m,0} = 1$ and $\tilde{m}_{1,0}$ evaluated with the ideal gases equation of state using $\tilde{p}_0 = 1$, $\tilde{T}_{m,0} = 1$.

In the simulation, $H_2$ was used as the working fluid, and its properties were taken from the technical literature [22]: $c_p = 14.510$ J/(kg K), $R = 4.124$ J/(kg K), $\mu = 1{,}25\ 10^{-5}$ kg/(m s). Additionally, the following values were used: $T_c = 300$ K, $\omega = 10\ \pi$ rad/s $= 3000$ rpm, $\alpha = 90°$ and $D_p = 0.1$ m.

Regarding the optimization of parameters, first a physical investigation is conducted to select the appropriate parameters to be optimized, which in the case of the present study was the pair $(\varphi, y)$. Therefore two levels of optimization were carried out in this study for maximum system efficiency. The ranges of variation of each parameter to be optimized were: $0.25 \leq \varphi \leq 0.7$ and $0.2 \leq y \leq 0.7$. The selected discretization in all ranges for the efficiency maximization was the coarsest set for which the optimal value of each parameter did not change as the sets became finer, while the relative error was kept below 1% in all cases [21].

## 4. Results

Initially, it was investigated the existence of optimal values for the volume parameters, $\sigma$, $\varphi$ and $x$, using the following values for the remaining parameters: $p^* = 10$ bar, $\beta = 2$, $\psi = 0{,}9$, $\tilde{A} = 25$, $y = 0.5$, $Z_1 = Z_2 = 400$, $\tilde{T}_h = 3$, $M^* = 8$ and $x = 0.5$. Notice that once, $\beta$ and $D_p$, are given, the reference volume $V^*$ can be computed. The total mass of gas can also be obtained from the specification of $p^*$, using Equation (25).

In order to indicate the validity of the assumptions, numerical procedure and engine characteristics, the analysis starts by presenting a $\tilde{p} \times \tilde{V}_t$ diagram, which is shown in Fig. 3a. The compression and expansion processes are clearly devised in the graphic, showing that a positive network is achieved. For the engine configuration simulated in Fig. 3, the efficiency was $\eta = 24.25$ %. Fig. 3b shows a $\tilde{p} \times \theta$ diagram, i.e., the behavior of the dimensionless indicated pressure with respect to crank angle during one engine cycle. Both graphs corroborate the expected trends for a Stirling engine, obtained with the simulations conducted with the mathematical model introduced in this paper.

As the percentage of the reference volume occupied by the total swept volume increases, $\sigma$ (0,80, 0,85 and 0,90), it is observed an increase in the cycle efficiency as shown in Fig. 4. This analysis illustrates the variation of the cycle efficiency against the parameter $\varphi$, that represents the fraction of the expansion swept volume with

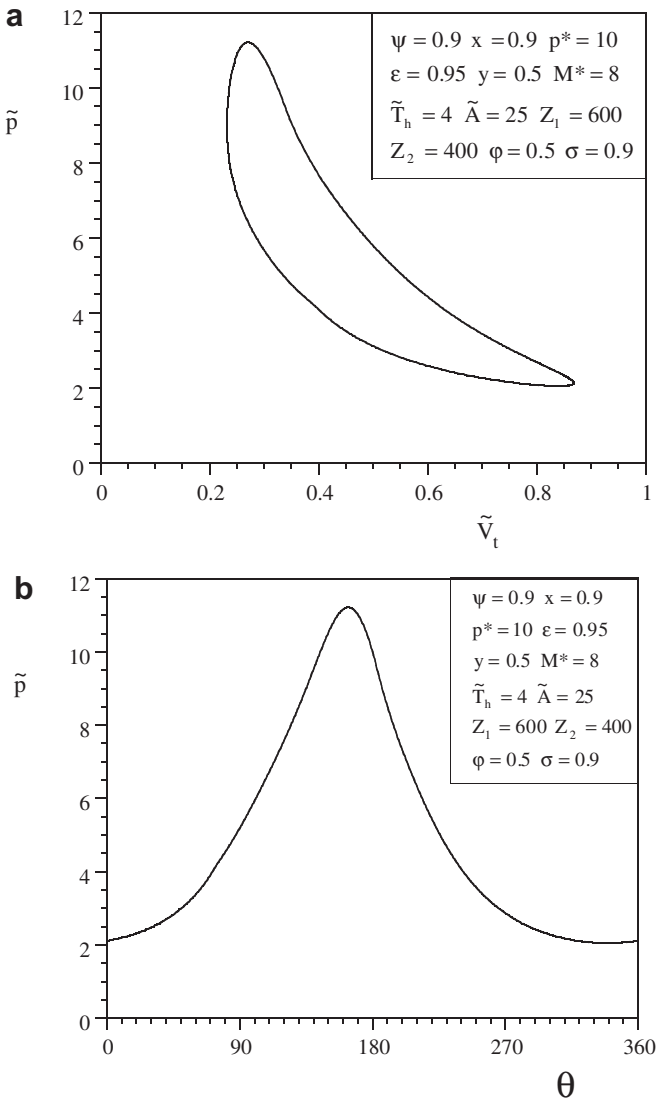


**Fig. 3.** (a) The $\tilde{p} \times \tilde{V}_t$ diagram of the double-acting swashplate Stirling engine, and (b) The $\tilde{p} \times \theta$ diagram of the double-acting swashplate Stirling engine.

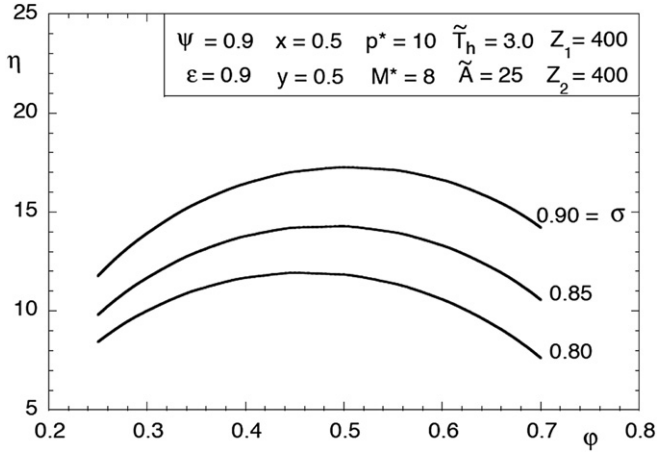


**Fig. 4.** Efficiency behavior with respect to $\varphi$, and varying $\sigma$.

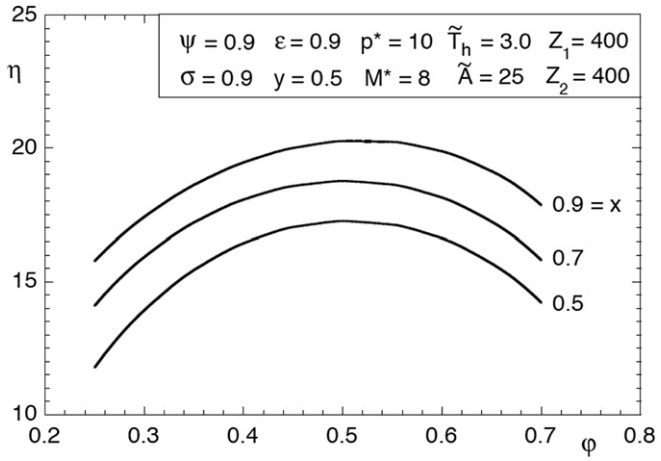


**Fig. 5.** Behavior of the efficiency $\eta$ with respect to $\varphi$, and varying $x$.

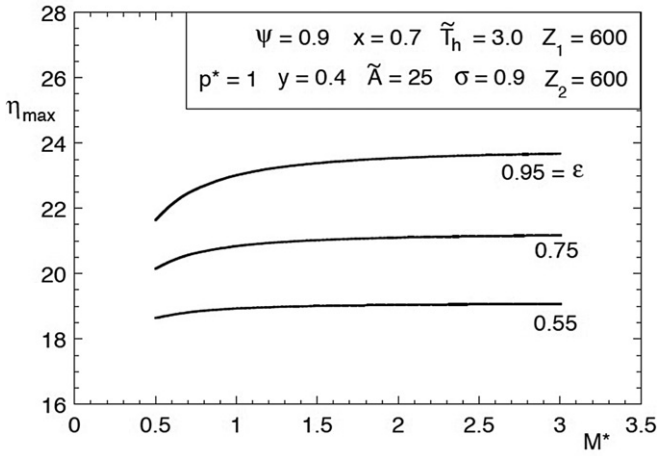


**Fig. 7.** Maximized efficiency, $\eta_{max}$, as a function of $M^*$, and varying $\varepsilon$.

respect to the total swept volume. With an equal allocation of volume to the heat exchangers $\tilde{V}_h$ and $\tilde{V}_c$, expressed by the parameter $x = 0.5$, it is observed a maximum efficiency corresponding to $\varphi \approx 0.5$, i.e., for equal swept volumes during compression and expansion. The optimal value of $\varphi$ decreases slightly for smaller values of $\sigma$.

Setting $\sigma = 0.9$, the search for higher efficiencies continues by varying the parameter $x$, i.e., by varying the volume distribution between the heat exchangers.

The simulation results are illustrated in Fig. 5. Higher efficiency values are obtained for larger values of $x$, i.e., when more volume is allocated to the hot end heat exchanger. It is important to note that $x = (\tilde{V}_h/\tilde{V}_h + \tilde{V}_c)$, therefore increasing $x$ does not imply in an increase of the hot side dead volume, which is known to be a negatively affecting factor in the performance of Stirling engines. Increasing $x$ means that more of the total available volume is allocated to the hot heat exchanger, therefore increasing the heat exchanger capability of collecting the available heat supply.

Once that the existence of a maximum efficiency corresponding to an optimal value of $\varphi_{opt} \cong 0.5$ was demonstrated, the model was used to study the effect of the parameters $Z_1$ and $Z_2$, that represent the length to diameter aspect ratio of the heat exchanger tubes. The results, shown in Fig. 6, indicate that larger values of these parameters increase the engine efficiency. This trend is justified due to the increase in the flow velocity inside the heat exchanger tubes (which increases the heat transfer coefficient) and, the resulting diameter reduction, due to the fixed heat exchange area constraint, i.e., for $y$ and $\tilde{A}$ fixed.

Fig. 7 illustrates the effect of the regenerator effectiveness, $\varepsilon$, on the maximized efficiency which increases as $\varepsilon$ increases, which is expected since more energy is captured for work conversion. The graph also illustrates by means of the parameter $M^*$, that the mass increase in the regenerator is unnecessary above $M^* \cong 1$.

Figs. (4)–(7) characterize the optimal value $\varphi_{opt} \cong 0.5$ as "robust", taking into consideration that it is insensitive to the variation of design parameters. This is valuable information from the point of view of engine design.

Fig. 8 illustrates a second geometric optimization opportunity for the cycle. It shows that the cycle efficiency can be maximized one more time, now with respect to the parameter $y$, which represents the percentage of heat transfer area of the hot side heat exchanger with respect to the total available heat transfer area. The graph also illustrates the variation of the parameter $p^*$, which is proportional to the total mass of working fluid used by the engine.

It is found that as the total mass of working fluid is reduced, the twice-maximized efficiency increases. It is observed that the optimal value $y_{opt} \cong 0.4$, is practically insensitive to variations of $p^*$. This finding is remarkable, as it characterizes the double optimization as "robust", i.e., independent of the main design parameters.

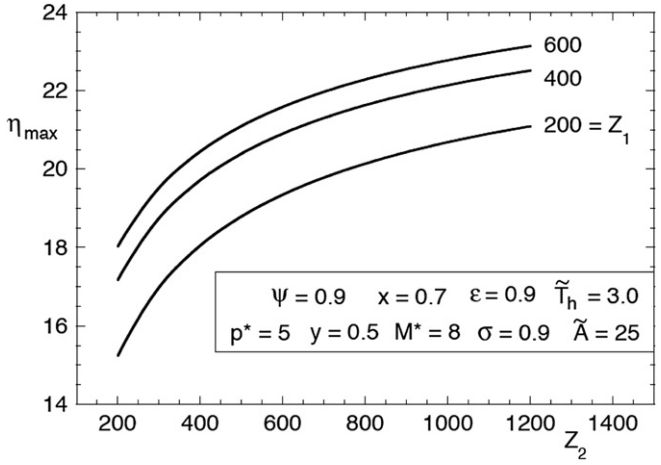


**Fig. 6.** Behavior of the maximized efficiency, $\eta_{max}$, with respect to $Z_2$, and varying $Z_1$.

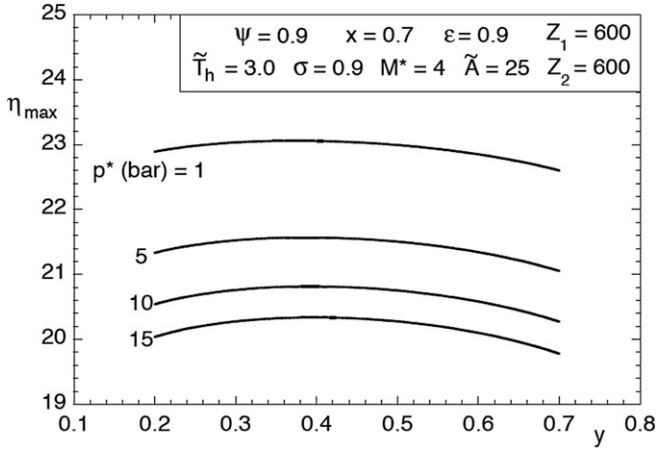


**Fig. 8.** Efficiency $\eta$ as a function of $y$ for variable $p^*$.

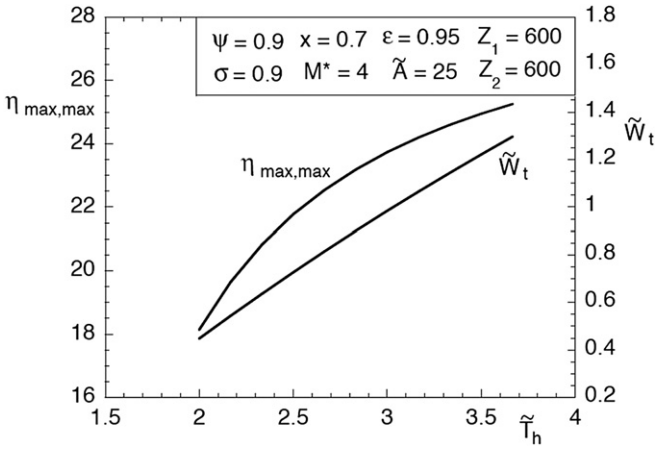


**Fig. 9.** Efficiency $\eta$ and work $\tilde{W}_t$ as functions of $\tilde{T}_h$.

Finally, the effect of varying the temperature of the hot source, $T_h$, in the twice-maximized cycle efficiency is considered. The results in Fig. 9 indicate an increase in the efficiency with the increase in the temperature of the hot source. Fig. 9 also illustrates the engine total work, $\tilde{W}_t$, that corresponds to the twice-maximized efficiency, as a function of $\tilde{T}_h$.

## 5. Conclusions

In this paper a mathematical model to simulate the operation of Stirling engines is introduced. A thermodynamic optimization of the cycle for maximum thermal efficiency is conducted. The numerical results show that there is an optimal engine geometry that maximizes the thermal efficiency. The results are reported using dimensionless variables, in normalized charts, which are general for the engine configuration considered, i.e., with a sliding disk mechanism ("swashplate").

The study identifies the location of the thermodynamic optima in terms of two important design parameters, $\varphi$ and $y$, and their sensitivity to other engine parameters. The thermodynamic optima are sharp, in the sense that a 225% variation of the calculated efficiency values was observed within the range of tested configurations in this study, and "robust" (i.e., relatively insensitive) to the variation of several parameters, e.g., $p^*$ (or $m_t$), $\tilde{T}_h$, $M^*$, $\varepsilon$, $Z_1$, $Z_2$, $x$ and $\sigma$. It is therefore reasonable to state that this conclusion is of great importance for engine design.

## Acknowledgements

The authors acknowledge with gratitude the support of the Center for Advanced Power Systems at Florida State University, AFOSR (Award No. FA9550-06-1-0527), the Brazilian National Council of Scientific and Technological Development, CNPq (project 554151/2010-3-CNPq), and the Engineering and Materials Science Graduate Program (PIPE) of the Federal University of Parana.

## References

[1] Moran MJ, Shapiro HN, Boettner DD, Bailey MD. Fundamentals of engineering thermodynamics. 7th ed. New York: John Wiley & Sons; 2011.
[2] Curzon FL, Ahlborn B. Efficiency of a Carnot engine at maximum power output. American Journal of Physics 1975;43:22–4.
[3] Reader GT, Hooper C. Stirling engines. 1st ed. London: E. & F. N. Spon; 1983.
[4] Urieli I, Berchowitz DM. Stirling cycle engine analysis. 1st ed. Bristol: Adam Hilger Ltd; 1984.
[5] Ladas HG, Ibrahim OM. Finite-time view of the Stirling engine. Energy 1994; 19(8):837–43.
[6] Blank DA, Wu C. Power optimization of an extraterrestrial solar-radiant Stirling heat engine. Energy 1995;20(6):523–30.
[7] Angelino G, Invernizzi C. Potential performance of real gas Stirling cycle heat pumps. International Journal of Refrigeration 1996;19(6):390–9.
[8] Popescu G, Radcenco V, Costea M, Feidt M. Finite-time thermodynamics optimisation of an endo- and exo-irreversible Stirling motor. Revue Generale de Thermique 1996;35(418–19):656–61.
[9] Erbay LB, Yavuz H. Analysis of the Stirling heat engine at maximum power conditions. Energy 1997;22(7):645–50.
[10] Bhattacharyya S, Blank DA. Design considerations for a power optimized regenerative endoreversible Stirling cycle. International Journal of Energy Research 2000;24(6):539–47.
[11] Senft JR. Optimum Stirling engine geometry. International Journal of Energy Research 2002;26(12):1087–101.
[12] Rogdakis ED, Bormpilas NA, Koniakos IK. A thermodynamic study for the optimization of stable operation of free piston Stirling engines. Energy Conversion and Management 2004;45(4):575–93.
[13] Tyagi SK, Lin G, Kaushik SC, Chen J. Thermoeconomic optimization of an irreversible Stirling cryogenic refrigerator cycle. International Journal of Refrigeration 2004;27(8):924–31.
[14] Mathieu A, Feidt M, Rochelle P, Grosu L, Gualino D, Grappe B. Preliminary sizing and optimization of a micro solar power plant by a parametric sensitivity study. Environmental Engineering and Management Journal 2010; 9(10):1381–7.
[15] Timoumi Y, Tlili I, Ben Nasrallah S. Design and performance optimization of GPU-3 Stirling engines. Energy 2008;33(7):1100–14.
[16] Timoumi Y, Tlili I, Ben Nasrallah S. Performance optimization of Stirling engines. Renewable Energy 2008;33(9):2134–44.
[17] Karabulut H. Dynamic analysis of a free piston Stirling engine working with closed and open thermodynamic cycles. Renewable Energy 2011;36(6):1704–9.
[18] Bejan A. Convection heat transfer. 2nd ed. New York: John Wiley & Sons; 1995.
[19] Reid RC, Prausnitz JM, Poling BE. Properties of gases and liquids. 4th ed. Boston: McGrawHill; 1987.
[20] Kincaid D, Cheney W. Numerical analysis. 1st ed. Belmont-CA: Wadsworth; 1991.
[21] Editorial. Journal of heat transfer editorial policy statement on numerical accuracy. ASME Journal of Heat Transfer 1994;116:797–8.
[22] Bejan A. Heat transfer. 1st ed. New York: John Wiley & Sons; 1993.

## Nomenclature

$A$: total heat transfer area, $A1 + A2$
$A_1$: heat transfer area in the expansion volume
$A_2$: heat transfer area in the compression volume
$a, b$: coefficients, Equations (15) and (16)
$c_p$: working fluid specific heat at constant pressure
$c_R$: regenerator specific heat
$c_v$: working fluid specific heat at constant volume
$D_1$: diameter of the tubes in the hot side heat exchanger
$D_2$: diameter of the tubes in the cold side heat exchanger
$h_1$: heat transfer convection coefficient in the expansion volume
$h_2$: heat transfer convection coefficient in the compression volume
$k$: gas thermal conductivity
$L_1$: length of the tubes in the hot side heat exchanger
$L_2$: length of the tubes in the cold side heat exchanger
$m_1$: mass in the expansion volume
$m_2$: mass in the compression volume
$m_R$: regenerator matrix mass
$m_t$: total working fluid (gas) mass
$N_1$: number of tubes in the hot side heat exchanger
$N_2$: number of tubes in the cold side heat exchanger
$Pr$: Prandtl number
$p$: internal pressure
$\dot{Q}_1$: heat transfer rate in the hot side heat exchanger
$\dot{Q}_2$: heat transfer rate in the cold side heat exchanger
$\dot{Q}_R$: heat transfer rate in the regenerator
$\tilde{Q}$: dimensionless heat transfer
$R$: gas constant
$Re_D$: Reynolds number based on internal tube diameter
$t$: time
$tol$: cycle convergence tolerance
$T_1$: temperature in the expansion volume
$T_2$: temperature in the compression volume
$T_c$: temperature of the cold reservoir,
$T_{c-1}$: conditional temperature that depends upon the gas flow direction and the heat exchange in the regenerator
$T_{c-2}$: conditional temperature that depends upon the gas flow direction and the heat exchange in the regenerator
$T_h$: temperature of the hot reservoir
$T_m$: temperature of the regenerator matrix
$T_R$: temperature of the gas leaving the regenerator
$u$: general unknown
$V_1$: total expansion volume
$V_2$: total compression volume
$V_c$: volume occupied by the cold heat exchanger
$V_{d-1}$: expansion dead volume

$V_{d-2}$: compression dead volume
$V_h$: volume occupied by the hot heat exchanger
$V_{s-1}$: total swept volume for expansion
$V_{s-2}$: total swept volume for compression
$w$: diameter ratio $\tilde{D}_1/\tilde{D}_2$
$\tilde{W}$: dimensionless cycle network
$x$: ratio between the hot side heat exchanger volume, $\tilde{V}_h$, and the total volume allocated to the heat exchangers, $(\tilde{V}_h + \tilde{V}_c)$
$y$: ratio between the heat transfer area of the hot side heat exchanger, $\tilde{A}_1$, and the total heat exchange area, $(\tilde{A}_1 + \tilde{A}_2) = \tilde{A}$
$Z_1$: length to diameter ratio for the tubes of the hot side heat exchanger
$Z_2$: length to diameter ratio for the tubes of the cold side heat exchanger

*Greek letters*
$\alpha$: phase angle
$\beta$: ratio between the reference volume V* and $\pi.D_p^3$
$\gamma$: specific heats ratio $c_p/c_v$
$\varepsilon$: regenerator effectiveness
$\varepsilon_{cycle}$: cycle relative error
$\eta$: cycle efficiency
$\theta$: crank angle, $\omega t \times 180/\pi$
$\sigma$: fraction of the reference volume, $V^*$, occupied by the total engine swept volume
$\varphi$: ratio between the total swept volume during the expansion, $\tilde{V}_{s-1}$, and the total swept volume, $(\tilde{V}_{s-1} + \tilde{V}_{s-2})$
$\psi$: ratio between the volume allocated to the heat exchangers, $(\tilde{V}_h + \tilde{V}_c)$, and the total dead volume, $(\tilde{V}_{d-1} + \tilde{V}_{d-2} + \tilde{V}_h + \tilde{V}_c)$
$\omega$: angular speed (rad/s)

*Subscripts*
*i used to represent the following:*
*s–1:* expansion swept volume
*s–2:* compression swept volume
*d–1:* dead expansion volume
*d–2:* dead compression volume
*c:* cold side heat exchanger
*h:* hot side heat exchanger
*1:* expansion space
*2:* compression space
*m:* regenerator matrix
*R:* fluid in the regenerator
*c–1:* conditional temperature in the expansion space
*c–2:* conditional temperature in the compression space
*max:* maximized (max, max = twice-maximized)
*t:* total

*Superscripts*
*: reference value (scale)
~: dimensionless variable